Universität Zürich

Physik-Institut

Characterization of the FBK VUV-HD 10×10 mm^2 SiPM

Astroparticle Physics Group
Frédéric Girard
08/05/2020

Universität Zürich[UZH]

1 Introduction

One of the most sensitive type of detector used in ultra-low background experiments are liquid noble gas Time-Projection Chambers [1, 2]. Some of these experiments, such as the current XENON [3], LUX [4], LUX-ZEPLIN [5], and the proposed DARWIN experiment [6], share a common design: a cylindrical field-cage, which ensures the production of a homogeneous electric field in the axial direction; two light sensing arrays, to allow for the detection of xenon scintillation light produced when a particle interacts with the liquid; and a cryostat, which keeps the xenon inside the detector in a liquid state ($\sim$ 170 K for liquid xenon).

For decades, the photosensor arrays have been composed of Photo-Multiplier Tubes (PMTs). These analog light sensors are well known for their high gain and low intrinsic noise level [7]. On the down side, these sensors are generally bulky, expensive, have a relatively poor photo-detection efficiency to VUV-light ($\sim$30%) and despite their good radiopurity, they are one of the major contributor to the material radioactivity of the detector [8].

As detectors get bigger and more sensitive, reducing the cost and increasing the radio-purity of sensor arrays is becoming of paramount importance. For this reason, we are characterizing Silicon Photo-Multipliers (SiPMs) in the search of a suitable candidate to replace PMTs for dark matter detectors.

The main characteristics SiPMs should have for low-energy searches are a low dark count rate, low cross-talk probability, high gain and a good VUV-sensitivity.

This report details the characterization of the 10×10 mm^2, 40 μm pitch , VUV-sensitive SiPM from the *Fondazione Bruno Kessler*. Section 2 presents the experimental setup and section 3 shows the breakdown voltage determination. Section 4 presents the gain, dark count rate and cross-talk analysis and section 5 shows our conclusions.

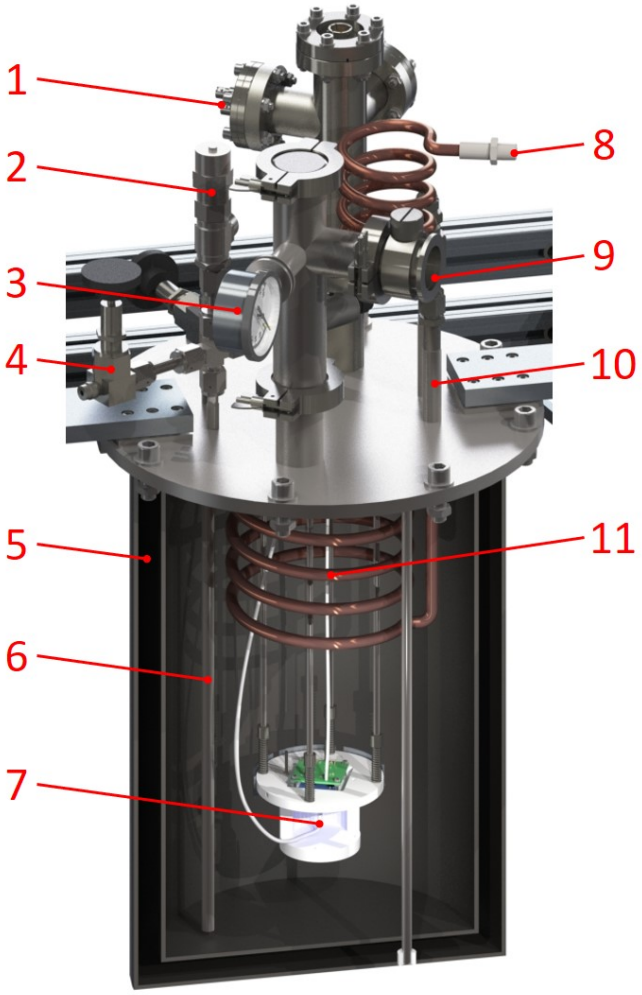

Figure 1 – Components view of LArS. The testing facility is made of an instrumented double-walled cryostat filled with GN_2. The temperature is controlled by adjusting the flow of LN_2 flowing in the cooling coil. Legend: 1 – Electrical and instrumentation feedthrough. 2 – Pressure relief valve. 3 – Manometer. 4 – GN_2 inlet. 5 – Cryostat. 6 – GN_2 outlet. 7 – SiPM cell. 8 – LN_2 outlet (solenoid valve not shown). 9 – Vacuum port. 10 – LN_2 inlet. 11 – Cooling coil. 12 – Support structure.

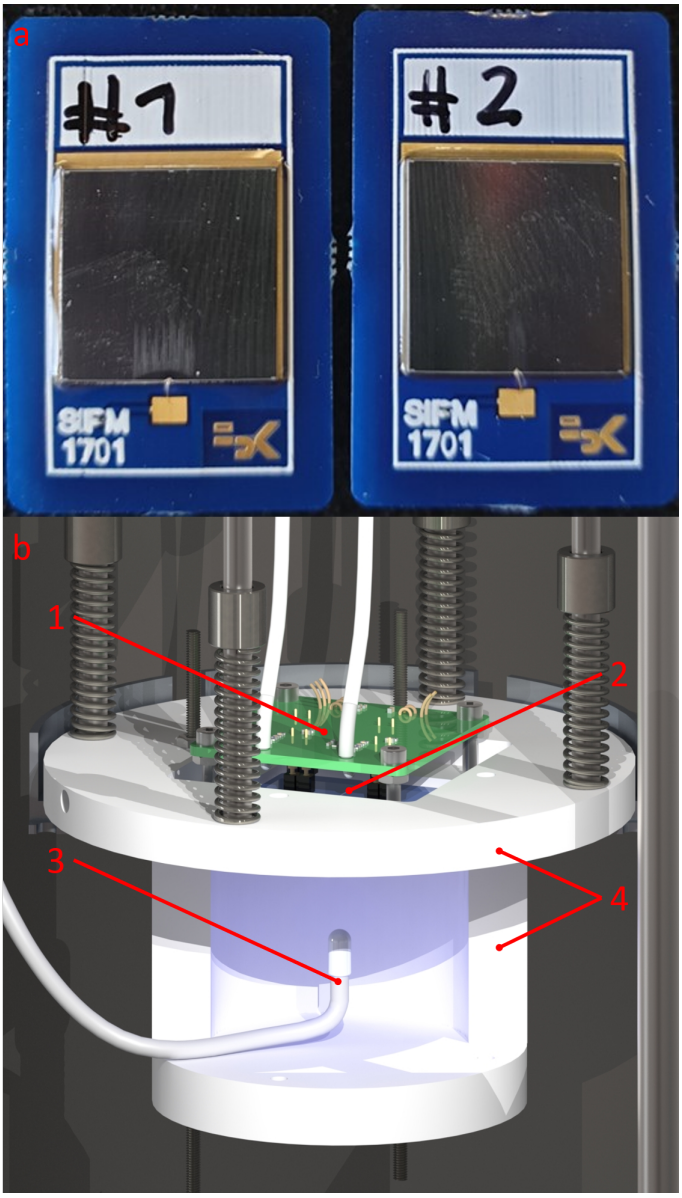

Figure 2 – a) Picture of two FBK VUV-HD 10×10 mm^2. b) LArS - SiPM cell. The SiPMs are mounted on a $\times$ 10 pre-amplified base and are down-looking toward a blue LED covered in thin PTFE tape (tape not shown). A PT100 thermistor (not shown) is located between the SiPMs and the pre-amplifier board to obtain accurate temperature readings of the sensors. Legend: 1 – $\times10$ pre-amplifier board. 2 – SiPMs. 3 – Blue LED. 4 – PTFE reflectors.

2 Experimental setup

The SiPMs were tested in the *Liquid Argon Setup* (LArS), at the University of Zürich. Previously used to test photosensors in liquid argon for the GERDA experiment [9], LArS has been re-purposed as a general photosensor testing facility. Figure 1 shows a schematic of the inner and outer components of the setup.

The main chamber consists of a vacuum insulated pressure vessel filled with gaseous nitrogen. A pressure relief valve allows us to set the pressure to 1.9 bar reliably. The GN_2 is cooled by flowing LN_2 in a copper pipe arranged in a coil.

A PID controller, receiving inputs from two PT100 sensors inside the pressure vessel, controls the flow of LN_2 by opening and closing a servo controlled valve at the LN_2 output. The temperature stability achieved throughout the measurement was within $\pm$ 0.1 K.

Inside the pressure vessel, a PTFE sensor cell hosts two SiPMs (see Figure 2). The two sensors showed a very similar behaviour, and to reduce the size of the data files, only one was used to when acquiring dark count data. The readout board with on-board $\times10$ pre-amplifier was designed by the electronic workshop of the physics department at UZH. An external $\times10$ amplifier brings the total amplification to $\times100$. A blue LED is located beneath the sensors and is used for calibration purposes, pulsed with a waveform generator. The SiPMs signals are recorded with a CAEN v1724 Analog-to-Digital Converter (ADC).

3 Breakdown Voltage Determination

Prior to any measurement at a new temperature, the breakdown voltage was measured. The blue LED was pulsed at 500 Hz with 60 *ns* square waveforms to illuminate the SiPMs with $\mathcal{O}(10-100)$ photo-electrons (p.e.). The intensity of the LED was kept constant

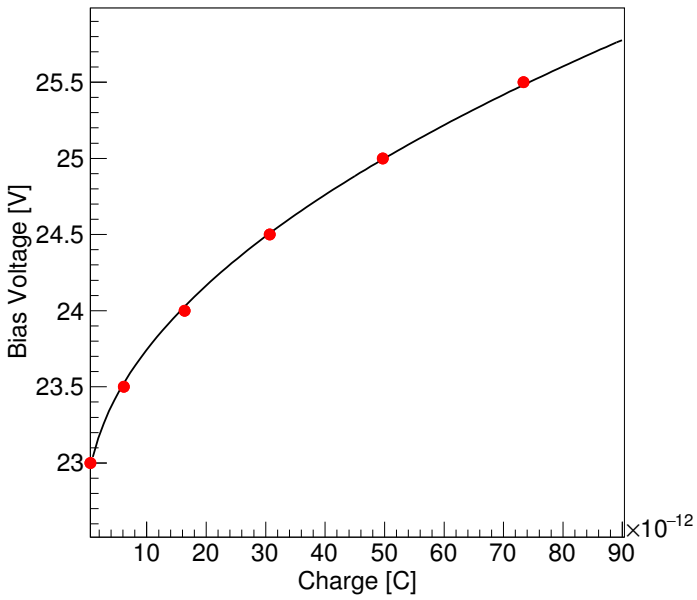

Figure 3 – Bias-voltage vs charge at 170 K. The y-intercept value is defined as the breakdown voltage. The black curve is a fit to the data with the formula from equation 2. The error on the bias voltage is $\pm$ 0.01 V. The error on the charge is obtained from the Gaussian fit of the charge distribution, and is small enough to be covered by the data points.

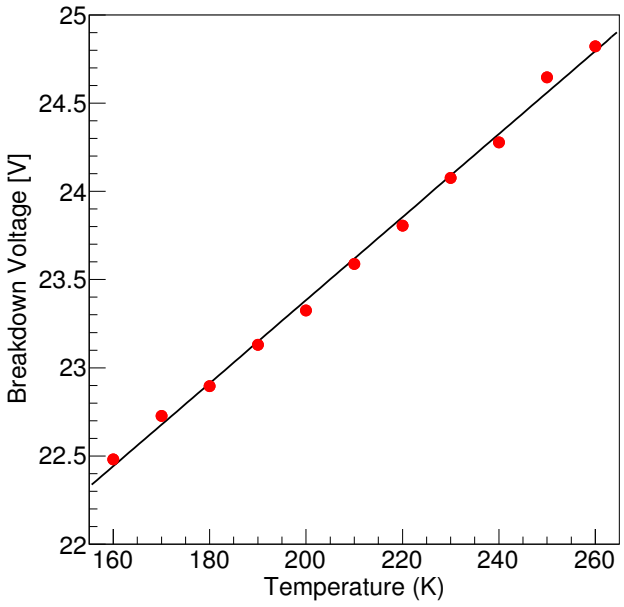

Figure 4 – Breakdown voltage vs temperature. The temperature stability is better than 0.1 K. The breakdown voltage decreases with temperature with a slope of (23.1 ± 0.1) mV/K

in order to ensure a constant illumination. Six bias voltages were arbitrarily selected just above the breakdown voltage and 200'000 pulses were recorded at each voltage. The raw data were processed with the Xurich-II processor, described in [10].

The ADC has a bandwidth of 10 MHz, recording the discrete voltage from the SiPM signal output every 10 *ns*. The processor identifies pulses and integrates them above a user defined threshold above the baseline. The integrated voltage can be converted to charge with the relation

$$q = \int I\,\mathrm{d}t = \frac{1}{R \cdot F_{amp}} \int V\,\mathrm{d}t = \frac{ADC_{range}}{R \cdot F_{amp} \cdot ADC_{res}} \int ADC_{level}\,\mathrm{d}t, \qquad (1)$$

where I is the current, R is the impedance of the ADC ($50\,\Omega$), F_{amp} is the amplification factor, V is the voltage, ADC_{level} is the level of the signal over 14 bits, ADC_{range} is the full range of the ADC (2.25 V), ADC_{res} is the resolution of the ADC (14 bit) and dt is the time resolution of the ADC of 10 *ns*.

We can fit the integrated peak area distribution (in ADC units) with a Gaussian function, taking the mean of the fit as the mean area of the pulses, then converting to charge. Figure 3 shows the bias-voltages associated with the charge produced in the SiPM at 170 K.

By definition, the breakdown voltage is the voltage at which no photo-avalanches are produced. We can directly determine this voltage by fitting the bias voltage vs charge with the formula:

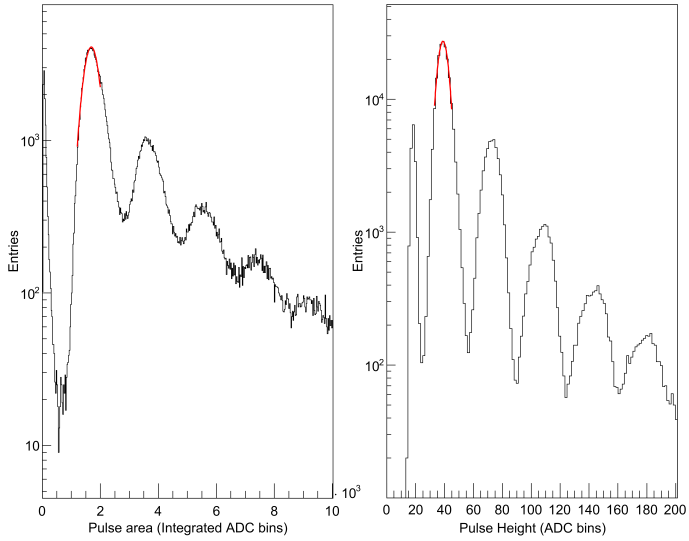

Figure 5 – Area and height SPE spectra at 190 K, 5V over-voltage. The 1.0 p.e peak is fitted with a Gaussian function (in red). The mean value of the fit is used to calculate the 1.0 p.e. value.

$$V_{bias} = V_{breakdown} + m \cdot \sqrt{q} \tag{2}$$

where m is a scaling factor. Figure 4 shows the breakdown voltage as a function of temperature where the black line is a linear fit.

4 Gain, Dark Count Rate and Cross-talk Probability

Dark count data (without LED pulses) was taken from 160 K to 210 K, as the dark count at higher temperatures were starting to exceed the bandwidth of the ADC. Dark count is characterized by non-correlated, low p.e. pulses. Figure 5 shows an example of the area and height single photo-electron (SPE) spectra, with 5V over-voltage, at 190 K. We used the dark count data to perform the gain calibration. We fitted the

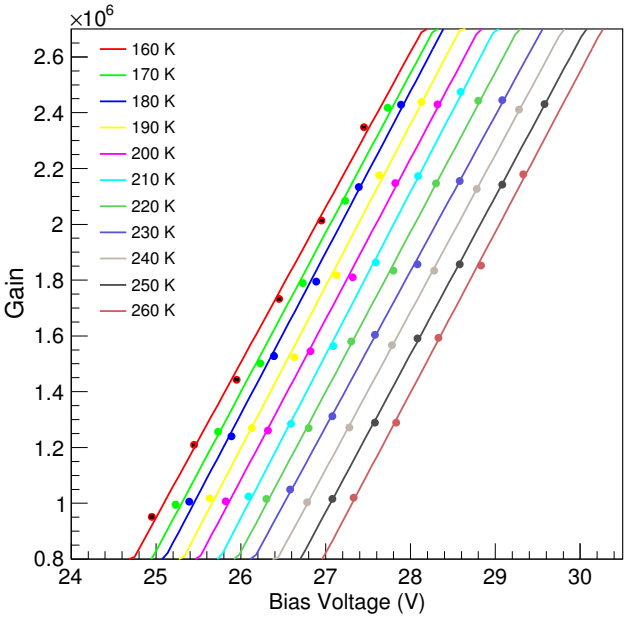

Figure 6 – Gain vs. bias voltage.

1 p.e. peak of the area SPE spectrum with a Gaussian function to determine the mean pulse area of the 1 p.e. peak. The gain is defined as:

$$G = q/Q \tag{3}$$

where q is the charge from equation 1 and Q is the elementary charge of the electron, $1.602176634 \cdot 10^{-19}$ C.

Figure 6 shows the gain as a function of the bias voltage for several temperatures. We obtained a gain of $\mathcal{O}(10^6)$, lower by a factor 2-5 to that of a typical VUV-sensitive PMT [7]. The $\times 10$ pre-amplifier we used allows us to detect 1 p.e. pulses nevertheless.

We define the Dark Count Rate (DCR) as the sum of uncorrelated pulses above a threshold of 0.5 p.e divided by the run time. In figure 7, we show the DCR obtained by varying the integration threshold. Having determined the 1 p.e. level by fitting the first peak, we can find the 0.5 and 1.5 p.e. level by looking for the

Sensor	Breakdown Voltage (V)	Operational Voltage (V)	Gain ($\times 10^6$)	DCR (Hz/mm^2)	DCR (Count/cell/day)	CTP (%)
FBK VUV-HD 10×10 mm^2	22.75	25.5-27.5	1.0 - 2.4	1.5 - 9.5	2.07 - 12.44	16-22
Hamamatsu VUV4 MPPC 6×6 mm^2 [11]	45.5	$\sim$ 54	$\sim$ 3.2	0.82	4.92	$\sim$ 4
Hamamatsu R11410-21 3" PMT [7]	-	$\sim$ 1500	$\sim$ 5	$\sim$ 0.01	N/A	N/A

Table 1 – Sensor Comparison. The DCR of the FBK 10×10 mm^2 SiPM is about 150 times greater than the one from the Hamamatsu R11410-21 3" PMT.

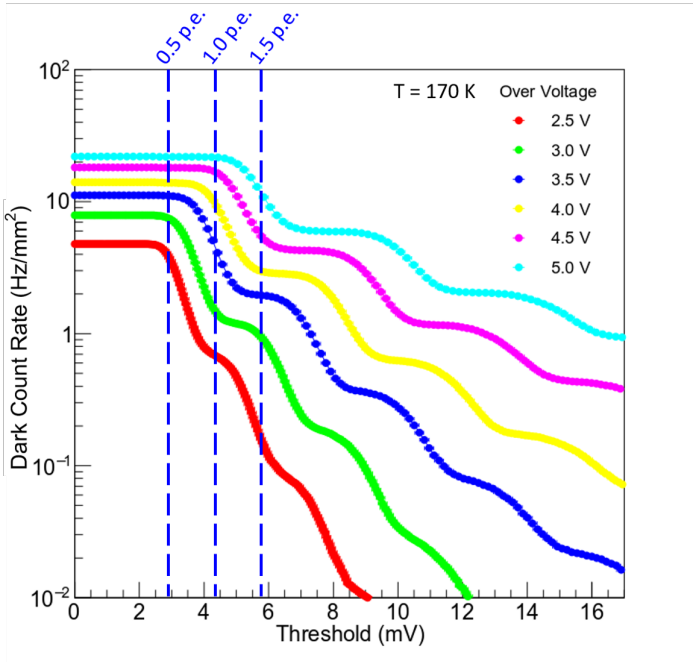

Figure 7 – Dark Count Rate vs. Integration threshold. The blue dashed lines indicate the 0.5, 1.0 and 1.5 p.e. thresholds for 3.5 V over-voltage

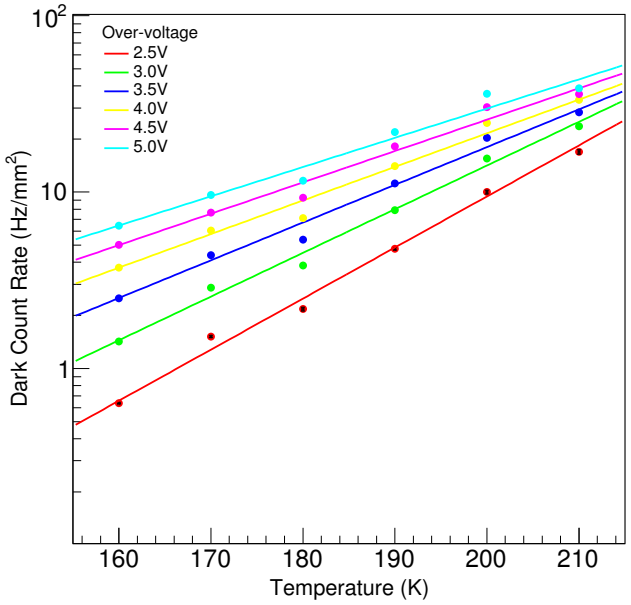

Figure 8 – Dark Count Rate vs. Temperature. At 170 K, the DCR is between 1.5 and 9.5 Hz/mm^2.

change in inflection in the curves left and right of the 1.0 p.e. threshold. As an example, the 0.5, 1.0 and 1.5 levels are indicated for the 3.5 V over-voltage in figure 7.

We then determined the DCR for all the data sets by integrating the entire photo-electron spectrum from the 0.5 p.e. level and divide by the full run time. The time stamp resolution of the DAQ is 1 second. Figure 8 shows the measured dark count rate as a function of temperature for over-voltage from 2.5 V

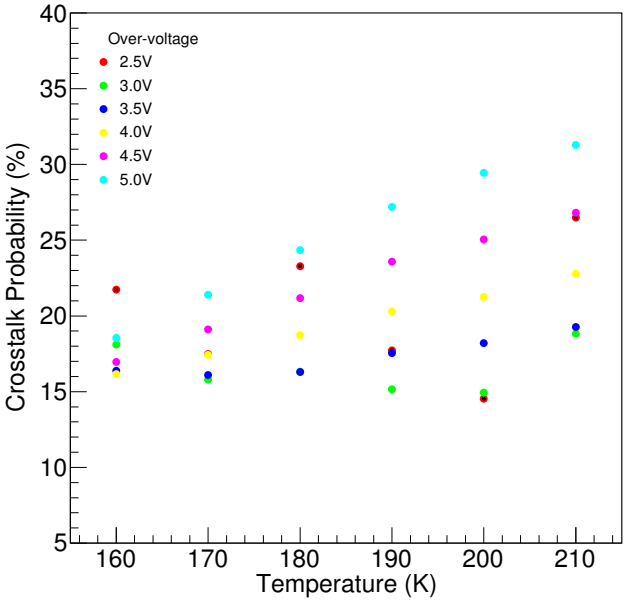

Figure 9 – Cross-Talk Probability vs. Temperature. At LXe temperature, we observe a CTP of about 16-22%. We observe an unusual temperature dependence of the cross-talk probability with temperature.

to 5.0 V. Close to the operating temperature of a liquid xenon TPC, 170 K, we observed a dark count rate of 1.5 Hz/mm^2 at 2.5 V over-voltage, about 150 times higher than Hamamatsu's 3" PMTs (R11410-21 [7]).

Finally, cross-talk is a phenomenon in which a photo-avalanche in a cell produced by a single photon produces secondary photons which are detected by neighboring cell with a certain probability. This cross-talk probability (CTP) is then defined as the ratio of the DCR at the 1.5 p.e. level and the DCR at the 0.5 p.e. level:

$$CTP = \frac{DCR_{1.5\ p.e.}}{DCR_{0.5\ p.e.}} \tag{4}$$

Figure 9 shows the CTP as a function of temperature. The CTP is usually temperature invariant, but in this measurement, we observed a temperature dependence at higher over-voltage. This could be due to some unidentified measurement artifact, or to a second order effect from this type of SiPM.

The results of this analysis are collected in table 1, along with results from two other studies performed at UZH, and published in [11] and [7] respectively. A direct comparison shows that the Hamamatsu VUV4 MPPC is performing slightly better than the FBK VUV-HD SiPM in gain and DCR. However, both sensors have gains lower, and DCR much higher, than the Hamamatsu R11410-21 3" PMT [7].

5 Conclusion

The testing of the FBK VUV-HD 10×10 mm^2 SiPM shows that this photosensor is still not suitable as a replacement to traditional PMTs for ultra-low background, low energy experiments. At liquid xenon temperature, the gain of the SiPM is still lower than that of the Hamamatsu R11410 by a factor 2 to 5, depending on the over-voltage. This is mitigated by the use of the $\times 10$ pre-amplifier and amplifier, which boost the signal voltage by a total factor of 100, facilitating the detection of SPEs.

The dark count rate is still much too high for low-energy searches with LXe, at $\mathcal{O}(1-10)$ Hz/mm^2, which would cause an accidental coincidence rate too elevated amongst the sensors. To achieve rates comparable to that of PMTs, the DCR should be reduced by 2 to 3 orders of magnitude. However, for high-energy searches such as for $0\nu\beta\beta$ decay of ^{136}Xe, a DCR lower than 50 Hz/mm^2 would be deemed sufficient [12], making this sensor a potential candidate. Finally, the CTP measured is compatible with other measurements, but the temperature dependence at higher over-voltages is still unexplained. This could be due to a measurement artifact or a second-order effects, which would need to be investigated.

We are planing on continuing the testing of SiPMs as manufacturers continue to improve their designs. The next sensors we will test are an improved version of the FBK VUV-HD, with an engineered electric field which is optimized for low temperatures, as well as a low DCR version of the Hamamatsu VUV-4 Multi Pixel Photon Counter.

References

[1] V. Chepel and H. Araújo, *Liquid noble gas detectors for low energy particle physics*, J. Inst. **8**, R04001 (2013), Publisher: IOP Publishing.

[2] E. Aprile and L. Baudis, Liquid noble gases, in *Particle Dark Matter: Observations, Models and Searches*, edited by G. Bertone, pp. 413–436, Cambridge University Press, 2010.

[3] X. Collaboration *et al.*, *The XENON1T Dark Matter Experiment*, Eur. Phys. J. C **77**, 881 (2017), arXiv: 1708.07051.

[4] C. F. P. da Silva, *Dark Matter Searches with LUX*, arXiv:1710.03572 [hep-ex, physics:physics] (2017), arXiv: 1710.03572.

[5] T. L. Collaboration *et al.*, *LUX-ZEPLIN (LZ) Conceptual Design Report*, arXiv:1509.02910 [astro-ph, physics:hep-ex, physics:physics] (2015), arXiv: 1509.02910.

[6] J. Aalbers *et al.*, *DARWIN: towards the ultimate dark matter detector*, J. Cosmol. Astropart. Phys. **2016**, 017 (2016), Publisher: IOP Publishing.

[7] P. Barrow, L. Baudis, D. Cichon, M. Danisch, D. Franco, F. Kaether, A. Kish, M. Lindner, T. M. Undagoitia, D. Mayani, L. Rauch, Y. Wei, and J. Wulf, *Qualification tests of the R11410-21 photomultiplier tubes for the XENON1T detector*, J. Inst. **12**, P01024 (2017), Publisher: IOP Publishing.

[8] E. Aprile *et al.*, *Physics reach of the XENON1T dark matter experiment.*, J. Cosmol. Astropart. Phys. **2016**, 027 (2016), Publisher: IOP Publishing.

[9] L. Baudis, G. Benato, R. Dressler, F. Piastra, I. Usoltsev, and M. Walter, *Enhancement of light yield and stability of radio-pure tetraphenyl-butadiene based coatings for VUV light detection in cryogenic environments*, J. Inst. **10**, P09009 (2015), Publisher: IOP Publishing.

[10] L. Baudis, Y. Biondi, M. Galloway, F. Girard, S. Hochrein, S. Reichard, P. Sanchez-Lucas, K. Thieme, and J. Wulf, *The first dual-phase xenon TPC equipped with silicon photomultipliers and characterisation with ^{37}Ar*, arXiv:2003.01731 [astro-ph, physics:hep-ex, physics:nucl-ex, physics:physics] (2020).

[11] L. Baudis, M. Galloway, A. Kish, C. Marentini, and J. Wulf, *Characterisation of Silicon Photomultipliers for liquid xenon detectors*, J. Inst. **13**, P10022 (2018), Publisher: IOP Publishing.

[12] G. Gallina *et al.*, *Characterization of the Hamamatsu VUV4 MPPCs for nEXO*, Nuclear Instruments and Methods in Physics Research Section A: Accelerators, Spectrometers, Detectors and Associated Equipment **940**, 371 (2019).